Volume 24, No 4 | International Journal of Radiation Research, October 2026

Radiation intensifies cyclophosphamide-associated ferroptosis-related changes in mouse spermatocyte-derived GC-2spd cells

H. Jin[1], Z. Xin[2], Q. Qian[1*], R. Han[1*]

[1]*Department of Prenatal Diagnosis, Xinjiang Uygur Autonomous Region Maternal and Child Health Hospital, Urumqi 830000, Xinjiang, China*
[2]*Department of Prenatal Diagnosis, Reproductive Medicine Center, The First Affiliated Hospital of Xinjiang Medical University, Urumqi 830000, Xinjiang, China*

► ***Original article***

Corresponding author:
Rui Han, Ph.D.,
Fang Qian, Ph.D.,
E-mail: *1f10547@xjmu.edu.cn, 13899852771@163.com*

Received: July 2025
Final revised: August 2026
Accepted: August 2026

Int. J. Radiat. Res., October 2026; 24(4): 1093-1099

DOI: 10.61186/ijrr.24.4.21

Keywords: *Cyclophosphamide, X-Rays, ferroptosis, spermatocytes.*

ABSTRACT

Background: To determine whether graded X-ray irradiation intensifies cyclophosphamide (CTX)-associated cytotoxic, oxidative, iron-related, and nuclear factor erythroid 2-related factor 2 (NRF2) and glutathione peroxidase 4 (GPX4) transcriptional changes in GC-2spd mouse spermatocyte-derived cells. ***Materials and Methods:*** GC-2spd cells were evaluated in three experimental series: CTX dose-response testing (0-400 µM), irradiation alone (0, 2, 4, or 8 Gy), and irradiation on a fixed 50 µM CTX background (0, 2, 4, or 8 Gy). For the fixed-CTX series, cells were exposed to CTX for 2 h before irradiation and maintained in CTX-containing medium for 48 h. All cellular, biochemical, and transcriptional endpoints were assessed 48 h after sham irradiation or irradiation. ***Results:*** CTX and X-ray irradiation each reduced cell viability in a concentration- or dose-dependent manner. On a fixed 50 µM CTX background, increasing radiation dose further reduced viability and increased apoptosis. Irradiation also increased malondialdehyde, total iron, and Fe^{2+} levels, decreased superoxide dismutase activity, and further reduced NRF2 and GPX4 mRNA expression in CTX-exposed cells, with the clearest changes at 4 and 8 Gy. These findings indicate ferroptosis-associated biochemical and transcriptional changes, but do not establish ferroptotic cell death or a CTX-radiation interaction. ***Conclusion:*** Graded X-ray irradiation intensified CTX-associated cytotoxicity, oxidative stress, iron dysregulation, and NRF2/GPX4 transcript suppression in GC-2spd cells. Direct lipid-peroxidation assays, protein-level pathway assessment, ferroptosis-rescue experiments, validated CTX bioactivation, and a factorial interaction design are required before causal ferroptosis or radiosensitization can be concluded.

INTRODUCTION

Cyclophosphamide (CTX) is a prodrug alkylating agent widely used to treat malignant and autoimmune diseases, while ionizing radiation remains a cornerstone of cancer therapy. Both modalities can impair male reproductive function, with reported consequences including reduced sperm counts, impaired motility, and infertility [1-4].

Reactive CTX metabolites, including acrolein, contribute to oxidative injury [5-7], whereas ionizing radiation causes direct macromolecular damage and generates reactive oxygen species (ROS), including through water radiolysis [8]. Although oxidative stress is well recognized in treatment-related gonadotoxicity, the contribution of non-apoptotic regulated cell-death pathways during combined exposure remains incompletely characterized.

Ferroptosis is a regulated form of cell death driven by iron-dependent phospholipid peroxidation and failure of cellular antioxidant defenses [9-11]. Ionizing radiation can trigger ferroptosis in tumor models [12-14], raising the question of whether related lipid-peroxidative injury also occurs in normal germ-cell systems. Nuclear factor erythroid 2-related factor 2 (NRF2) coordinates antioxidant and iron-handling programs, whereas glutathione peroxidase 4 (GPX4) limits phospholipid hydroperoxide accumulation [15-17]. Altered *NRF2/GPX4* signaling may therefore accompany ferroptosis susceptibility, although transcript measurements alone do not establish pathway activity or ferroptotic cell death.

Ferroptosis has been implicated in cisplatin-induced Sertoli-cell injury [18] and in radiation responses in other cell systems [19]. However, whether graded ionizing radiation intensifies CTX-associated ferroptosis-related alterations in spermatocyte-derived cells remains unclear. The novelty of the present study lies in integrating graded X-ray irradiation with a fixed CTX exposure in GC-2spd cells and simultaneously characterizing cytotoxicity, apoptosis, oxidative-stress indices, cellular iron status, and *Nfe2l2/Gpx4* transcriptional responses. This approach provides a cell-specific framework for examining whether irradiation aggravates the oxidative and iron-related phenotype associated with

[Downloaded from ijrr.com on 2026-11-08]

[DOI: 10.61186/ijrr.24.4.21]

CTX exposure in spermatocyte-derived cells. Accordingly, we first characterized the individual CTX and radiation dose responses and then evaluated graded irradiation in cells maintained on a fixed 50 μM CTX background. The study was designed as an exploratory in vitro assessment of ferroptosis-associated changes rather than a definitive demonstration of ferroptotic cell death, pharmacologic synergy, or radiosensitization.

MATERIALS AND METHODS

Cell culture and experimental treatments

Procell Life Science & Technology Co., Ltd. (Wuhan, China) provided the mouse spermatocyte-derived GC-2spd cell line, which was utilized as an in vitro model. High-glucose Dulbecco's modified Eagle medium (DMEM; Gibco, Thermo Fisher Scientific, Waltham, MA, USA) supplemented with 10% fetal bovine serum and 1% penicillin-streptomycin (Gibco, Thermo Fisher Scientific, Waltham, MA, USA) was used to cultivate the cells at 37°C in a humidified 5% CO2 incubator. After cell confluence reached 80%–90%, cells were detached for culturing using 0.25% trypsin (Gibco, Thermo Fisher Scientific, USA). Cells in the logarithmic growth phase were sown at the proper density and left to adhere overnight prior to experimental treatment.

To determine appropriate cyclophosphamide (CTX) concentrations, a preliminary dose-range experiment was conducted using CTX (HY-17420, MedChemExpress, USA) at 0, 25, 50, 100, 200, and 400 μM for 48 h. At the end of the 48-h treatment period, cell viability was assessed using the Cell Counting Kit-8 (CCK-8; FC101-03, TransGen Biotech Co., Ltd., Beijing, China), and the half-maximal inhibitory concentration (IC_{50}) was calculated. Based on the results, formal experiments included CTX at 25, 50, and 100 μM.

For irradiation experiments, cells were plated overnight before treatment and then exposed to X-rays using an X-RAD 320 irradiator (Precision X-Ray Inc., USA) at a dose rate of 2 Gy/min at room temperature. Doses of 0 (sham-irradiated control), 2, 4, and 8 Gy were delivered. Immediately after irradiation, cells were returned to the incubator and maintained for 48 h before outcome assessment.

For the fixed-CTX irradiation experiments, cells were exposed to 50 μM CTX for 2 h before irradiation at 0 (sham), 2, 4, or 8 Gy. Following irradiation, cells were maintained in CTX-containing medium for an additional 48 h, after which the specified cellular, biochemical, and transcriptional endpoints were assessed. CTX is a prodrug that requires metabolic activation; the bioactivation capacity of GC-2spd cells was not verified in this study, so the observed effects may reflect limited conversion to active metabolites. Because a full CTX-by-radiation factorial design was not employed, no formal synergy or interaction was inferred. When appropriate, the control group was subjected to sham irradiation and fed complete medium containing an equivalent volume of sterile normal saline. There were at least three separate biological replicates in each experimental group. There were no human subjects nor live animals involved.

Post-treatment sample collection and outcome measurements

At the end of the 48-hour post-treatment period, cell viability was assessed using the Cell Counting Kit-8 (CCK-8; FC101-03, TransGen Biotech Co., Ltd., Beijing, China). GC-2spd cells were seeded in 96-well plates at a density of 5×10^3 cells/well in 100 μL of complete medium per well prior to treatment. Cells were allowed to adhere overnight before treatment. Following the designated treatments, 10 μL of CCK-8 reagent was added to each well, and the plates were incubated at 37°C for two hours. The absorbance at 450 nm was measured using a microplate reader (BioTek Instruments, USA). Wells containing growth medium and CCK-8 reagent but devoid of cells were called blanks. Relative cell viability was calculated using the formula cell viability (%) = [(A_treated − A_blank)/(A_control − A_blank)] × 100. The mean value of the technical replicates was used for each independent biological experiment.

For apoptosis analysis, cells were harvested 48 h after treatment. Both floating and adherent cells were collected to minimize the loss of detached apoptotic cells; adherent cells were detached using 0.25% trypsin without EDTA. The collected cells were washed twice with cold phosphate-buffered saline (PBS) and resuspended in 1× Annexin V binding buffer at a concentration of approximately 1×10^6 cells/mL. An aliquot of 100 μL of the cell suspension (approximately 1×10^5 cells) was transferred to a flow-cytometry tube, followed by the addition of 5 μL of PE-conjugated Annexin V and 5 μL of 7-aminoactinomycin D (7-AAD) from the PE Annexin V Apoptosis Detection Kit I (Cat. No. 559763, BD Biosciences, USA). Samples were gently mixed and incubated for 15 min at room temperature in the dark. Subsequently, 400 μL of 1× binding buffer was added to each tube, and samples were analyzed within 1 h using a FACSCalibur flow cytometer (BD Biosciences, USA).

Unstained cells and single-stained controls were used to establish fluorescence compensation and quadrant boundaries. A minimum of 10,000 events was acquired per sample after exclusion of debris based on forward- and side-scatter characteristics. Data were analyzed using CellQuest Pro software (BD Biosciences, USA). PE Annexin V-negative/7-AAD-negative cells were considered viable, whereas PE Annexin V-positive/7-AAD-negative cells were classified as early apoptotic cells. The reported total

[Downloaded from ijrr.com on 2026-11-08]

[DOI: 10.61186/ijrr.24.4.21]

apoptotic fraction was calculated as the sum of early and late apoptotic/Annexin V-positive populations.

For biochemical analyses, cells were collected 48 h after treatment, resuspended in PBS, lysed by sonication on ice using a sonicator, and centrifuged at 12,000 × g for 10 min at 4°C using a refrigerated centrifuge. The resulting supernatants were used for biochemical measurements. To measure the amount of malondialdehyde (MDA), the thiobarbituric acid reactive compound method (A003-1-2) was used (Nanjing Jiancheng Bioengineering Institute, Nanjing, China). In order to assess the activity of total superoxide dismutase (T-SOD), a T-SOD assay kit (A001-3-1, Nanjing Jiancheng Bioengineering Institute, Nanjing, China) was used. A total cellular iron measurement kit (E-BC-K880-M, Elabscience Biotechnology Co., Ltd., Wuhan, China) and a ferrous iron measurement kit (E-BC-K881-M, Elabscience Biotechnology Co., Ltd., Wuhan, China) were used according to the manufacturer's instructions. To normalize the protein quantity, bicinchoninic acid (BCA) protein assay kit (P0011, Beyotime Biotechnology, Shanghai, China) was used.

Total ribonucleic acid (RNA) was extracted from cell pellets using TRIzol reagent (Invitrogen, Thermo Fisher Scientific, Carlsbad, CA, USA) in accordance with the manufacturer's instructions for gene-expression analysis. The cells were harvested 48 hours after treatment. A NanoDrop 2000 spectrophotometer (Thermo Fisher Scientific, USA) was used to measure the RNA content and purity. samples with an A260/A280 ratio between 1.8 and 2.0. were applied to the reverse transcription that followed. Agarose-gel electrophoresis was used to evaluate RNA integrity.Using 5X All-In-One RT Master Mix (G492, Applied Biological Materials [ABM], Canada), first-strand complementary DNA (cDNA) was created from 1 μg of total RNA using the following program: 25°C for 10 minutes, 42°C for 50 minutes, and 85°C for 5 minutes.

EvaGreen Express 2× qPCR Master Mix-Low Rox (G891, Applied Biological Materials [ABM], Canada) was used for real-time quantitative PCR on a LightCycler® 480 System (Roche, Switzerland). Each reaction comprised 10 μL of 2× qPCR MasterMix, 0.6 μL of 10 μM forward primer, 0.6 μL of 10 μM reverse primer, 1 μL of cDNA template, and nuclease-free water to a final volume of 20 μL for the 20-μL reaction setup. The cycling regimen comprised 40 cycles of 95°C for 15 seconds and 60°C for 60 seconds after an initial denaturation at 95°C for 10 minutes. The amplification specificity was then evaluated using a melting-curve analysis from 65°C to 95°C. Each assay had to have a single dominating melting peak in order to be accepted. All reactions were performed in triplicate.

Quantification cycle (Ct) values obtained from technical triplicates were averaged for each biological replicate before subsequent calculations. Expression of the target genes was normalized to the reference gene Actb. For each sample, ΔCt was calculated as Ct_target − Ct_Actb. The ΔΔCt value was then calculated as ΔCt_treated − ΔCt_calibrator, and relative gene expression was expressed as 2^{-}ΔΔCt. For irradiation-only experiments, the sham-irradiated 0-Gy group served as the calibrator and was assigned a relative expression value of 1. For the fixed-CTX irradiation experiments, the 50 μM CTX plus sham-irradiation group served as the calibrator and was assigned a value of 1. Technical replicates were averaged before statistical analysis, and independent biological replicates constituted the statistical unit.

Primer sequences, RefSeq accession numbers, and corresponding amplicon sizes are presented in table 1. All primers were synthesized by Sangon Biotech Co., Ltd. (Shanghai, China).

Table 1. Primer sequences used for quantitative real-time PCR.

Gene	RefSeq accession	Forward primer (5′→3′)	Reverse primer (5′→3′)	Product size (bp)
Nfe2l2	NM_010902.4	CAGCATAGAGCAGGACATGGAG	GAACAGCGGTAGTATCAGCCAG	107
Gpx4	NM_008162.4	GCAATGAGGCAAAACTGACG	CTTGATTACTTCCTGGCTCCTG	131
Actb	NM_007393.5	AAGAGCTATGAGCTGCCTGA	TACGGATGTCAACGTCACAC	160

Statistical analysis

The information is displayed as mean ± standard deviation (SD). GraphPad Prism 9.0 (GraphPad Software, San Diego, CA, USA) was used for all statistical analyzes. One-way analysis of variance (ANOVA) was used to compare various groups, and Tukey's post-hoc test was used for pairwise comparisons. Before ANOVA, normality and homogeneity of variance were assessed using the Shapiro-Wilk test and Levene's test, respectively. Each experiment employed at least three different biological replicates, and the technical replicates were averaged. $P < 0.05$ was regarded as statistically significant, and all tests were two-tailed. No formal interaction or synergy analysis was carried out as the combination groups were not created using a complete factorial design.

RESULTS

CTX and radiation reduce cell viability

The 48-h CTX concentration-response experiment yielded an estimated IC_{50} of 109.3 μM (figure 1A). CTX at 25, 50, and 100 μM progressively reduced cell viability relative to vehicle control (figure 1B). In the irradiation-only experiment, cell viability was assessed 48 h after sham irradiation (0 Gy) or exposure to 2, 4, or 8 Gy. Compared with the 0-Gy sham-irradiated, non-irradiated reference group, irradiation caused a dose-dependent reduction in cell viability, with the 8-Gy group retaining approximately 48% of the sham-control value (figure 1C). These results confirm that both modalities produce graded

[Downloaded from ijrr.com on 2026-11-08]

[DOI: 10.61186/ijrr.24.4.21]

cytotoxicity in GC-2spd cells, providing a basis for the fixed-CTX combination experiments described below.

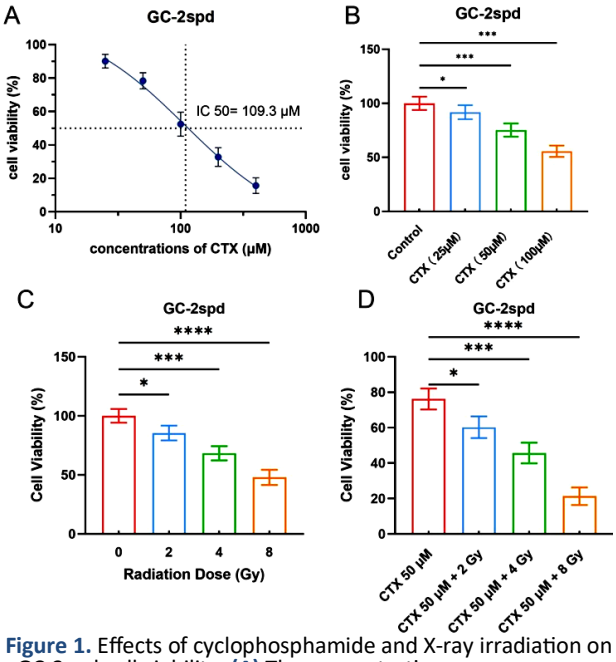


Figure 1. Effects of cyclophosphamide and X-ray irradiation on GC-2spd cell viability. **(A)** The concentration-response curve for cyclophosphamide (CTX) after 48 hours of exposure to 0, 25, 50, 100, 200, or 400 μM CTX; the estimated half-maximal inhibitory concentration (IC_{50}) was 109.3 μM. **(B)** Relative cell viability following exposure to 0, 25, 50, or 100 μM CTX for 48 hours. **(C)** Relative cell viability assessed 48 hours following X-ray irradiation at 2, 4, or 8 Gy or sham irradiation (0 Gy; non-irradiated reference). **(D)** Relative cell viability in cells exposed to a fixed dose of 50 μM CTX evaluated 48 hours after sham irradiation or irradiation at 2, 4, or 8 Gy. The Cell Counting Kit-8 (CCK-8) test was used to measure cell viability, which was then expressed in relation to the appropriate control group. Data are presented as mean ± standard deviation (SD); n = 5 independent biological replicates for panels A and B and n = 3 independent biological replicates for panels C and D. In panel B, *P < 0.05 and ***P < 0.001 versus the vehicle control. In panels C and D, *P < 0.05, ***P < 0.001, and ****P < 0.0001 versus the first group within the corresponding panel.

Radiation increases cytotoxicity and apoptosis

On a fixed 50 μM CTX background, cell viability was assessed 48 h after sham irradiation or exposure to 2, 4, or 8 Gy. Relative to the 50 μM CTX plus sham-irradiation group, which served as the non-irradiated reference, 2, 4, and 8 Gy progressively reduced cell viability, with the greatest reduction observed after 8 Gy (figure 1D). Because the fixed-CTX series did not include a complete factorial comparison, these data demonstrate an irradiation dose response in CTX-exposed cells but do not establish a CTX-radiation interaction.

Apoptosis was quantified 48 h after sham irradiation or irradiation on the fixed 50 μM CTX background. Compared with the 50 μM CTX plus sham-irradiation reference group, the apoptotic fraction increased progressively after 2, 4, and 8 Gy, with the largest increases observed after 4 and 8 Gy (figure 2A and B). Thus, apoptosis contributes to the radiation-associated loss of viability in CTX-exposed cells and should be distinguished mechanistically from ferroptotic cell death.

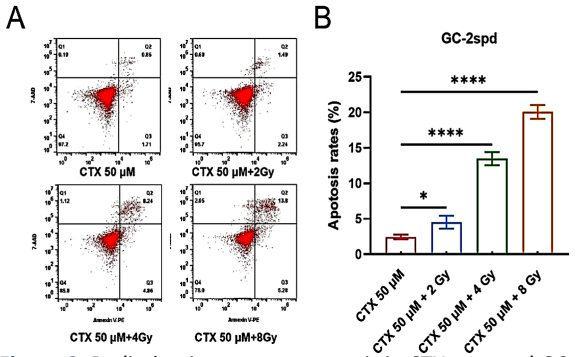


Figure 2. Radiation increases apoptosis in CTX-exposed GC-2spd cells. GC-2spd cells were kept in CTX-containing media for an extra 48 hours after being subjected to 50 μM cyclophosphamide (CTX) for two hours prior to sham irradiation (0 Gy) or X-ray irradiation at 2, 4, or 8 Gy. Phycoerythrin-conjugated Annexin V (Annexin V-PE) and 7-aminoactinomycin D (7-AAD) were used in flow cytometry to measure apoptosis. **(A)** Typical flow-cytometry plots of Annexin V-PE/7-AAD from the 50 μM CTX + sham, CTX + 2 Gy, CTX + 4 Gy, and CTX + 8 Gy groups. **(B)** Using the gating technique outlined in the Methods, the overall apoptotic fraction 48 hours after irradiation was determined from the Annexin V-positive apoptotic populations. The non-irradiated reference group was the 50 μM CTX plus sham-irradiation group. Data are presented as mean ± SD from three independent biological replicates (n = 3). *P < 0.05 and ****P < 0.0001 versus the 50 μM CTX plus sham-irradiation group.

Radiation increases oxidative stress and iron dysregulation

Biochemical endpoints were measured 48 h after sham irradiation or irradiation. In the irradiation-only experiment, the 2-Gy group did not differ significantly from the 0-Gy sham-irradiated reference group in MDA content, SOD activity, total iron, or Fe^{2+} levels, whereas 4 and 8 Gy increased MDA, total iron, and Fe^{2+} and decreased SOD activity. On the fixed 50 μM CTX background, the same endpoints were assessed 48 h after sham irradiation or exposure to 2, 4, or 8 Gy. Relative to the 50 μM CTX plus sham-irradiation reference group, 2 Gy produced no significant change in these four indices, whereas 4 and 8 Gy increased MDA, total iron, and Fe^{2+} and decreased SOD activity (figure 3A–D). The largest changes occurred after 8 Gy. These findings indicate irradiation dose-related oxidative stress and iron dyshomeostasis that are compatible with, but not specific to, ferroptosis.

Radiation suppresses Nfe2l2 and *Gpx4 expression*

Gene-expression measurements were performed 48 h after sham irradiation or irradiation. In the irradiation-only experiment, Nfe2l2 mRNA expression was reduced after 2, 4, and 8 Gy relative to the 0-Gy sham-irradiated reference group, whereas Gpx4 mRNA expression was significantly reduced after 4 and 8 Gy. On the fixed 50 μM CTX background, *Nfe2l2* and *Gpx4* mRNA expression was assessed 48 h after sham irradiation or exposure to 2, 4, or 8 Gy. Relative to the 50 μM CTX plus sham-irradiation reference group, increasing irradiation dose progressively reduced Nfe2l2 and Gpx4 mRNA expression (figure 4A and B), with the most pronounced reductions observed after 8 Gy. These transcriptional changes

[Downloaded from ijrr.com on 2026-11-08]

[DOI: 10.61186/ijrr.24.4.21]

accompanied the oxidative and iron-related phenotype; however, mRNA levels alone do not confirm suppression of *NRF2/GPX4* pathway activity protein abundance, *NRF2* nuclear localization, *GPX4* enzymatic activity, or functional rescue data would be required for that conclusion.

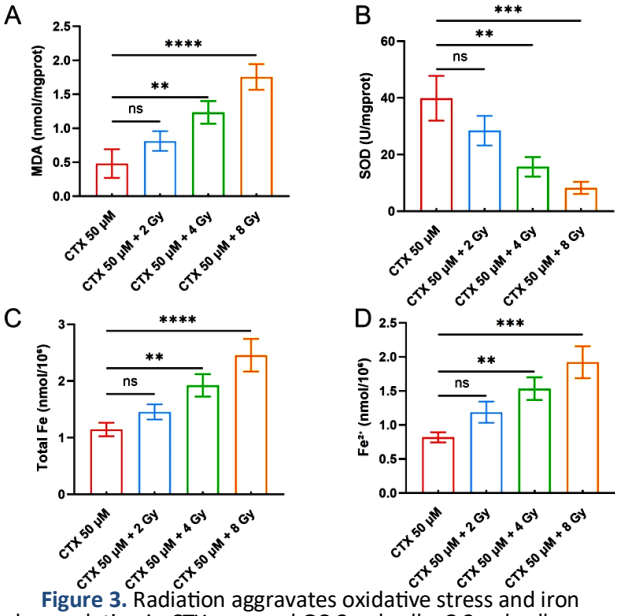


Figure 3. Radiation aggravates oxidative stress and iron dysregulation in CTX-exposed GC-2spd cells. C-2spd cells were kept in CTX-containing media for an extra 48 hours after being exposed to 50 μM cyclophosphamide (CTX) for two hours prior to either sham irradiation (0 Gy) or X-ray irradiation at 2, 4, or 8 Gy. Malondialdehyde (MDA) content, superoxide dismutase (SOD) activity, total cellular iron, and ferrous iron (Fe^{2+}) levels were examined 48 hours after irradiation. Total iron and Fe2+ readings were normalized to cell number, while MDA and SOD values were standardized to total protein content. The non-irradiated reference group was the 50 μM CTX plus sham-irradiation group. Three independent biological replicates (n = 3) of the data are displayed as mean ± SD. ns, not significant; **P < 0.01, ***P < 0.001, and ****P < 0.0001 versus the 50 μM CTX plus sham-irradiation group.

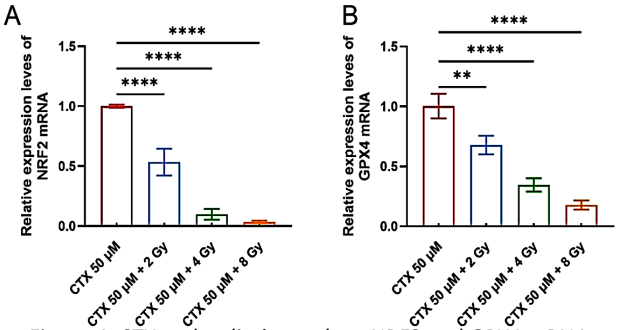


Figure 4. CTX and radiation reduce NRF2 and GPX4 mRNA levels in GC-2spd cells. GC-2spd cells were kept in CTX-containing media for an extra 48 hours after being subjected to 50 μM cyclophosphamide (CTX) for two hours prior to sham irradiation (0 Gy) or X-ray irradiation at 2, 4, or 8 Gy. 48 hours after radiation, the relative mRNA expression of (A) Nfe2l2 and (B) Gpx4 was assessed by quantitative real-time PCR. With the 50 μM CTX plus sham-irradiation group acting as the non-irradiated calibrator and a relative expression value of 1, expression was normalized to Actb (β-actin) and computed using the $2^{-}\Delta\Delta Ct$ technique. Three independent biological replicates (n = 3) of the data are displayed as mean ± SD. ****P < 0.0001 and **P < 0.01 in comparison to the 50 μM CTX with sham-irradiation group.

DISCUSSION

Taken together, the observed pattern is consistent with an oxidative and iron-dysregulation phenotype that may increase susceptibility to ferroptosis; however, the current endpoints are insufficient to establish ferroptotic cell death [20-25].

Recent studies in spermatocyte models provide biological support for this interpretation. Wang *et al.* reported iron overload and lipid peroxidation in spermatocytes following PM2.5 exposure, with cellular injury attenuated by deferoxamine and ferrostatin-1, whereas Li *et al.* demonstrated ferroptosis-associated spermatogenic injury in GC-2spd cells involving functional regulation of GPX4 [26, 27]. Therefore, rather than being evidence of ferroptotic cell death, the current findings should be understood as ferroptosis-associated alterations [19].

The increase in Fe^{2+} provides a plausible biochemical route to lipid peroxidation through iron-catalyzed radical generation [28-30]. In parallel, reduced GPX4 transcripts may indicate diminished antioxidant capacity.

Consistent with this interpretation, a recent study of ionizing-radiation injury in endothelial cells linked ferroptosis-related damage to alterations in MDA, SOD, Fe^{2+}, and the SLC7A11/GPX4 antioxidant system; importantly, that study also incorporated protein-level and ferroptosis-modulating evidence beyond bulk oxidative-stress markers [31, 32].

The dose-dependent changes observed after adding irradiation to a fixed CTX background suggest that radiation aggravates the cellular phenotype under these conditions. However, the design does not compare all CTX and radiation dose combinations within a single factorial experiment; it therefore cannot distinguish independent radiation effects from a true CTX-by-radiation interaction, nor can it establish additivity, synergy, or radiosensitization.

An important methodological consideration is that CTX is a prodrug whose canonical cytotoxicity depends on metabolic activation to 4-hydroxycyclophosphamide and downstream reactive metabolites [21]. In a recent study, Liao *et al.* demonstrated CTX-associated ferroptotic injury in Leydig cells and showed that ferrostatin-1 and deferoxamine attenuated CTX-induced testicular and Leydig-cell abnormalities [22]. This provides evidence linking CTX exposure to ferroptosis-related reproductive injury, but it does not resolve the bioactivation issue in the GC-2spd monoculture used here. The metabolic capacity of GC-2spd cells was not established in the present study. The observed concentration-response relationship confirms exposure-associated effects but does not identify the active chemical species. Future experiments should verify CTX bioactivation in this system or use a defined active metabolite such as

[Downloaded from ijrr.com on 2026-11-08]
[DOI: 10.61186/ijrr.24.4.21]

4-hydroperoxycyclophosphamide, with matched solvent and handling controls.

Recent evidence specifically from spermatocytes strengthens the mechanistic relevance of GPX4. Li *et al.* reported that triptolide promoted GPX4 degradation in mouse spermatocytes and GC-2spd cells; GPX4 deletion aggravated ferroptotic injury, whereas GPX4 overexpression mitigated it [27]. In contrast, the present study measured only Gpx4 mRNA, and reduced transcript abundance cannot establish reduced GPX4 protein content or enzymatic activity.

Direct assessment of lipid peroxidation - for example, using the lipid peroxidation-sensitive fluorescent probe C11-BODIPY 581/591 - together with rescue by ferrostatin-1, liproxstatin-1, or an iron chelator, is required to determine whether the loss of viability is ferroptosis dependent. Demonstrating involvement of the NRF2/GPX4 axis would require assessment of NRF2 nuclear localization, NRF2 and GPX4 protein levels, downstream targets such as SLC7A11, GCLC, and ferritin, and preferably gain- or loss-of-function rescue experiments [15, 16, 33].

The coexistence of reduced antioxidant capacity and increased cellular iron is biologically coherent with greater susceptibility to lipid peroxidation. Nevertheless, SOD activity and bulk iron measurements cannot identify the membrane phospholipid species involved or establish the lethal lipid-peroxidation threshold characteristic of ferroptosis. These biochemical measurements should therefore be integrated with direct lipid-ROS assays and cell-death rescue experiments.

Similar radiation-associated shifts in oxidative balance have been reported in IJRR studies. Kamal El-Dein and Anees observed increased lipid-peroxidation indices together with reduced antioxidant defenses following γ-irradiation-induced testicular injury, while Ogbanya *et al.* reported dose-related reductions in SOD, GPx, and CAT and increased MDA after CT radiation exposure [4, 34].

Clinically, chemotherapy and radiotherapy can both contribute to gonadal injury [1, 3, 20, 25], but the present single-cell-line model does not reproduce hepatic CTX metabolism, the testicular microenvironment, fractionated radiotherapy, or clinical exposure schedules. The current findings identify a candidate mechanism for further study rather than a basis for recommending ferroptosis-directed fertility protection.

This study has several limitations. It used one immortalized mouse spermatocyte-derived cell line and did not reproduce the testicular microenvironment, Sertoli-cell support, the blood-testis barrier, or in vivo pharmacokinetics. CTX bioactivation was not verified. Ferroptosis-specific rescue, direct lipid-ROS measurements, ultrastructural assessment, and NRF2/GPX4 protein or activity assays were not performed. The fixed-CTX irradiation series lacked a complete factorial design and could not test interaction or radiosensitization. Apoptosis after irradiation alone was not quantified in the current dataset. In addition, all cellular, biochemical, and transcriptional endpoints were assessed at a single 48-h post-treatment time point, precluding evaluation of the temporal sequence and persistence of the observed changes. These limitations preclude causal claims regarding ferroptosis, *NRF2/GPX4* signaling, or CTX-radiation interaction.

CONCLUSION

In summary, CTX and X-rays both caused dose-dependent cellular damage, and the effects of graded radiation were potentiated in the presence of a 50 μM CTX background, as evidenced by cytotoxicity, oxidative stress, iron-mediated changes, and NRF2/GPX4 transcriptional changes. The findings suggest the need for future studies on ferroptosis as a possible mechanism for CTX/radiation-induced spermatocyte cell death. To make definitive conclusions regarding the mechanisms of action, CTX activation must be verified along with the following:

Acknowledgments: *None*.
Conflict of Interest Statement: The authors declare no competing interests.
Funding: This work was supported by the Xinjiang Uygur Autonomous Region Natural Science Foundation (Grant No. 2023D01C232).
Ethics approval: Not applicable. This study used an established mouse spermatocyte cell line and involved no live animals or human participants.
Author contributions: H.J.: Conceptualization, data curation, formal analysis, investigation, methodology, writing – original draft. Z.X.: Data curation, formal analysis, investigation, validation, writing – review & editing. Q.F.: Supervision, resources, writing – review & editing. R.H.: Conceptualization, project administration, resources, supervision, validation, writing – review & editing. All authors read and approved the final manuscript.
Data availability: The raw data supporting the findings of this study, including uncropped flow-cytometry files and qPCR raw Ct values, are available from the corresponding author upon reasonable request.
Declaration of generative AI and AI-assisted technologies in the writing process: During the revision of this manuscript, the authors used AI-Assisted Technologies to assist with language editing, grammatical refinement, and improvement of clarity and organization. The tool was not used to generate experimental data, perform statistical analyses, or independently interpret the study findings. All AI-assisted content was critically reviewed, verified, and edited by the authors, who take full responsibility for

[Downloaded from ijrr.com on 2026-11-08]
[DOI: 10.61186/ijrr.24.4.21]

the accuracy, integrity, and final content of the manuscript.

REFERENCES

1. Perez-Garcia LF, Dolhain RJEM, Vorstenbosch S, *et al.* (2020) The effect of paternal exposure to immunosuppressive drugs on sexual function, reproductive hormones, fertility, pregnancy and offspring outcomes: a systematic review. *Hum Reprod Update,* ***26****(6): 961-1001*.
2. Ahmed AR and Hombal SM (1984) Cyclophosphamide (Cytoxan): A review on relevant pharmacology and clinical uses. *J Am Acad Dermatol,* ***11****(6): 1115-1126*.
3. Okada K and Fujisawa M (2019) Recovery of spermatogenesis following cancer treatment with cytotoxic chemotherapy and radiotherapy. *World J Mens Health,* ***37****(2): 166-174*.
4. Kamal El-Dein EKE and Anees LM (2020) Ameliorative role of melatonin against cypermethrin or gamma irradiation induced testicular damage in male rats. *Int J Radiat Res,* ***18****(4): 765-776*.
5. Yang Y, Zhang Z, Zhang H, *et al.* (2017) Effects of maternal acrolein exposure during pregnancy on testicular testosterone production in fetal rats. *Mol Med Rep,* ***16****(1): 491-498*.
6. Vivarelli F, Canistro D, Cirillo S, *et al.* (2019) Impairment of testicular function in electronic cigarette (e-cig, e-cigs) exposed rats under low-voltage and nicotine-free conditions. *Life Sci,* ***228****: 53-65*.
7. Jiang X, Ren Z, Zhao B, *et al.* (2020) Ameliorating effect of pentadecapeptide derived from Cyclina sinensis on cyclophosphamide-induced nephrotoxicity. *Mar Drugs,* ***18****(9): 462*.
8. Azzam EI, Jay-Gerin JP, Pain D (2012) Ionizing radiation-induced metabolic oxidative stress and prolonged cell injury. *Cancer Lett,* ***327****(1-2): 48-60*.
9. Dixon SJ, Lemberg KM, Lamprecht MR, *et al.* (2012) Ferroptosis: an iron-dependent form of nonapoptotic cell death. *Cell,* ***149****(5): 1060-1072*.
10. Wang H, Liu C, Zhao Y, *et al.* (2020) Mitochondria regulation in ferroptosis. *Eur J Cell Biol,* ***99****(1): 151058*.
11. Yang H, Chen X, Huang S, *et al.* (2026) A novel GSH depletor for simultaneous ferroptosis and cuproptosis activation in hepatocellular carcinoma. *Biochem Pharmacol,* ***243****: 117488*.
12. Li X, Liao X, Chen W, *et al.* (2026) Paeonol inhibits cell growth by inducing ferroptosis in human glioma cells. *Pharmacol Res Perspect,* ***14****(1): e70213*.
13. Lei G, Zhang Y, Koppula P, *et al.* (2020) The role of ferroptosis in ionizing radiation-induced cell death and tumor suppression. *Cell Res,* ***30****(2): 146-162*.
14. Lang X, Green MD, Wang W, *et al.* (2019) Radiotherapy and immunotherapy promote tumoral lipid oxidation and ferroptosis via synergistic repression of SLC7A11. *Cancer Discov,* ***9****(12): 1673-1685*.
15. Abdelgawwad El-Sehrawy AAM, Al-Dulaimi AA, Alkhathami AG, *et al.* (2025) NRF2 as a ferroptosis gatekeeper in colorectal cancer: implications for therapy. *Naunyn Schmiedebergs Arch Pharmacol,* ***398****: 16479-16506*.
16. Dodson M, Castro-Portuguez R, Zhang DD (2019) NRF2 plays a critical role in mitigating lipid peroxidation and ferroptosis. *Redox Biol,* ***23****: 101107*.
17. Ursini F and Maiorino M (2020) Lipid peroxidation and ferroptosis: the role of GSH and GPx4. *Free Radic Biol Med,* ***152****: 175-185*.
18. Fan Z, Xin P, Zhao L, *et al.* (2024) Ferroptosis is crucial for cisplatin induced Sertoli cell injury via N6-methyladenosine dependent manner. *World J Mens Health,* ***42****(4): 865-880*.
19. Ye LF, Chaudhary KR, Zandkarimi F, *et al.* (2020) Radiation-induced lipid peroxidation triggers ferroptosis and synergizes with ferroptosis inducers. *ACS Chem Biol,* ***15****(2): 469-484*.
20. Abdi M, Fadaee M, Jourabchi A, *et al.* (2024) Cyclophosphamide-induced infertility and the impact of antioxidants. *Am J Reprod Immunol,* ***92****(6): e70014*.
21. Emadi A, Jones RJ, Brodsky RA (2009) Cyclophosphamide and cancer: golden anniversary. *Nat Rev Clin Oncol,* ***6****(11): 638-647*.
22. Liao S, Wei C, Wei G, *et al.* (2024) Cyclophosphamide activates ferroptosis-induced dysfunction of Leydig cells via SMAD2 pathway. *Biol Reprod,* ***110****(5): 1012-1024*.
23. Selvakumar E, Prahalathan C, Mythili Y, *et al.* (2004) Protective effect of DL-alpha-lipoic acid in cyclophosphamide induced oxidative injury in rat testis. *Reprod Toxicol,* ***19****(2): 163-167*.
24. Wang Y, Zou Z, Jaisi A, *et al.* (2021) Unravelling the protective effects of emodin against cyclophosphamide induced gonadotoxicity in male Wistar rats. *Drug Des Devel Ther,* ***15****: 4403-4411*.
25. Ding J, Wang H, Wu ZB, *et al.* (2015) Protection of murine spermatogenesis against ionizing radiation-induced testicular injury by a green tea polyphenol. *Biol Reprod,* ***92****(1): 6*.
26. Wang J, Zhang Z, Shi F, *et al.* (2023) PM2.5 caused ferroptosis in spermatocyte via overloading iron and disrupting redox homeostasis. *Sci Total Environ,* ***872****: 162089*.
27. Li J, Chen D, Suo J, *et al.* (2024) Triptolide induced spermatogenesis dysfunction via ferroptosis activation by promoting K63-linked GPX4 polyubiquitination in spermatocytes. *Chem Biol Interact,* ***399****: 111130*.
28. Carocci A, Catalano A, Sinicropi MS, *et al.* (2018) Oxidative stress and neurodegeneration: the involvement of iron. *Biometals,* ***31****(5): 715-735*.
29. Saad HM, Salem EA, Elhussieny O, *et al.* (2025) Crosstalk between ferroptosis and miRNA in type 2 diabetes mellitus and possible therapeutic targeting. *Eur J Med Res,* ***30****(1): 982*.
30. Latunde-Dada GO (2017) Ferroptosis: role of lipid peroxidation, iron and ferritinophagy. *Biochim Biophys Acta Gen Subj,* ***1861****(8): 1893-1900*.
31. Wen L, Zhang W, Hu J, *et al.* (2024) Luteolin target HSPB1 regulates endothelial cell ferroptosis to protect against radiation vascular injury. *PLoS One,* ***19****(10): e0311922*.
32. Ma N, Hu W, Deng Y, Yuan L, Sun Y (2026) Carbon ions collapse the hypoxic lipid shield to decouple survival from redox vulnerability in NSCLC. *Free Radic Biol Med,* ***252****: 400-410*.
33. Ma H and Wu CY (2026) Improving oxidative stress and radiation-induced injury in diminished ovarian reserve rats by warming needle moxibustion via Keap1-Nrf2-ARE pathway. *Int J Radiat Res,* ***24****(2): 435-439*.
34. Ogbanya K, Mgbe E, Modebe E, Abah I, Nnaji T (2024) Effects of different doses of computed tomography radiation on the oxidation markers, antioxidant enzymes, and lipid profiles of male albino rats. *Int J Radiat Res,* ***22****(3): 631-637*.

[Downloaded from ijrr.com on 2026-11-08]

[DOI: 10.61186/ijrr.24.4.21]

[DOI: 10.61186/ijrr.24.4.21] [Downloaded from ijrr.com on 2026-11-08]